Mesothelial fusion mediates chorioallantoic membrane formation

Hiroki Nagai[1], Yuki Tanoue[1], Tomonori Nakamura[2,3,4], Christopher J. J. Chan[1,5], Shigehito Yamada[6], Mitinori Saitou[2,3,7], Takaichi Fukuda[8] and Guojun Sheng[1,*]

1: International Research Center for Medical Sciences (IRCMS), Kumamoto University, Kumamoto, Japan

2: Institute for the Advanced Study of Human biology (WPI-ASHBI), Kyoto University, Japan

3: Department of Anatomy and Cell Biology, Graduate School of Medicine, Kyoto University, Kyoto, Japan

4: The Hakubi Center for Advanced Research, Kyoto University, Kyoto, Japan

5: Current affiliation: Francis Crick Institute, London, UK

6: Congenital Anomaly Research Center, Kyoto University Graduate School of Medicine, Kyoto, Japan

7: Center for iPS Cell Research and Application (CiRA), Kyoto University, Kyoto, Japan.

8: Department of Anatomy and Neurobiology, Graduate School of Medical Sciences, Kumamoto University, Kumamoto, Japan

* Corresponding author: sheng@kumamoto-u.ac.jp

Abstract

In amniotic vertebrates (birds, reptiles and mammals), an extraembryonic structure called chorioallantoic membrane (CAM) functions as respiratory organ for embryonic development. The CAM is derived from fusion between two pre-existing membranes, the allantois, a hindgut diverticulum and a reservoir for metabolic waste, and the chorion which marks the embryo's external boundary. Modified CAM in eutherian mammals, including the human, gives rise to chorioallantoic placenta. Despite its importance, little is known about cellular and molecular mechanisms mediating CAM formation and maturation. In this work, using the avian model, we focused on the early phase of CAM morphogenesis when the allantois and chorion meet and initiate fusion. We report here that chicken chorioallantoic fusion takes place when the allantois reaches the size of 2.5-3.0mm in diameter and in about six hours between E3.75 and E4. Electron microscopy and immunofluorescence analyses suggested that before fusion, in both the allantois and chorion, an epithelial-shaped mesothelial layer is present, which dissolves after fusion, presumably by undergoing epithelial-mesenchymal transition. The fusion process per se, however, is independent of allantoic growth, circulation, or its connection to the developing mesonephros. Mesoderm cells derived from the allantois and chorion can intermingle post-fusion, and chorionic ectoderm cells exhibit a specialized sub-apical intercellular interface, possibly to facilitate infiltration of allantois-derived vascular progenitors into the chorionic ectoderm territory for optimal oxygen transport. Finally, we investigated chorioallantoic fusion-like process in primates, with limited numbers of archived human and fresh macaque samples. We summarize the similarities and differences of CAM formation among different amniote groups, and propose that mesothelial epithelial-mesenchymal transition mediates chorioallantoic fusion in most amniotic vertebrates. Further study is needed to clarify tissue morphogenesis leading to chorioallantoic fusion in primates. Elucidating molecular mechanisms regulating mesothelial integrity and epithelial-mesenchymal transition will also help understand mesothelial diseases in the adult, including mesothelioma, ovarian cancer and fibrosis.

Introduction

Placentation in eutherian mammals is mediated through a specialized fetomaternal interface that facilitates exchanges of oxygen, nutrients and metabolic byproducts between two circulatory systems that do not physically meet (Carter, 2012; Mossman, 1987). The anatomical basis of chorioallantoic placenta, the main type of eutherian placentas, is chorioallantoic membrane (CAM), which functions as a respiratory organ in birds, reptiles, and primitive mammals (Mossman, 1987). The CAM is derived from fusion between the chorion and allantois, two extraembryonic tissues present in all amniotic vertebrates (Sheng and Foley, 2012), including in some marsupial clades which primarily utilize choriovitelline placentas (another major mode of placentation) for fetomaternal exchanges (Carter, 2021; Mossman, 1987). The chorion is composed of an ectoderm layer and an extraembryonic somatic mesoderm layer (Fig.1A). The allantois has an endoderm layer originated as a hindgut diverticulum and is covered by a complex layer of vascularized extraembryonic splanchnic mesoderm (Fig.1A). Extraembryonic coelomic cavity, the space between the allantois and chorion, is gradually displaced by the expanding allantois and after chorioallantoic fusion, by the expanding chorioallantoic membrane (CAM). In birds, the CAM eventually grows to cover the entire undersurface of egg shell. Several studies have investigated the process of mammalian allantoic bud outgrowth (Downs and Rodriguez, 2020; Hassan and Viebahn, 2017). However, little is known about morphogenetic or molecular features during CAM fusion or its subsequent maturation into a functional placenta. In a systematic genetic study in mice (Perez-Garcia et al., 2018), placental abnormalities were reported to account for two thirds of embryonic lethal mutations, a finding that highlights the need to gain a better understanding of how the CAM/placenta forms and matures to be the largest and most important organ during amniote development (Rossant and Cross, 2001).

In this work, we used the avian model and studied early CAM morphogenesis, focusing on a 12-hour window (E3.75 to E4.25) from before the chorioallantoic fusion to soon after the initiation of CAM formation. We show that chorioallantoic fusion takes place within six hours after the chorion and allantois

come into contact at E3.75 and when the allantois reaches a size of approximately 2.5mm in diameter. Chorioallantoic fusion, however, is independent of allantoic size increase or allantoic circulation. We also show that both chorionic and allantoic mesothelial cells are of epithelial organization and that chorioallantoic fusion is associated with a partial epithelial-mesenchymal transition behavior. Electron microscopy analysis reveals an unexpected complexity of intercellular junctional interactions between chorionic ectoderm cells, likely in preparation for intra-ectodermal invasion of vascular progenitors soon after CAM establishment, an evolutionarily conserved feature to minimize physical distance between embryonic red blood cells and the external environment for efficient transport of oxygen and other small molecules (Coleman and Terepka, 1972; Hoshi and Mori, 1971). Finally, we present CAM-related data in primate embryos, obtained from historically archived early human embryo sections and freshly collected macaque embryo samples.

Results and Discussion

Chorioallantoic fusion takes place between E3.75-E4.25

Chicken allantois starts to emerge from the hindgut and extends into the extraembryonic coelomic cavity at the end of the third day of incubation, when the developing embryo is completely enclosed by amniotic membrane, and reaches the chorion by the fifth day of incubation (Hirota, 1894; Romanoff, 1960; Steinmetz, 1930). To better understand the timing of CAM fusion, we used a custom-built whole-egg incubation device for time-lapse imaging (Fig.1B,C), and captured tissue morphogenesis of the chicken embryo from E2 to E5 (Sup-Mov.1; this movie was generated by the corresponding author and is also available in a public depository with the following link: https://www.sdbcore.org/object?ObjectID=354). Still images from the movie (Fig.1E) revealed rapid increase of allantoic size during this period of development. The endoderm-enclosed allantoic cavity could be visualized by fast green dye injection

(Fig.1D) and the injected dye did not leak into the extraembryonic coelomic cavity, suggesting that allantoic endoderm as an epithelial barrier was functional before chorioallantoic fusion. Backflow of the dye into the embryo proper was not prominent either, suggesting that expansion of the allantoic cavity during its rapid growth phase was not due to functional maturation of embryonic mesonephros.

We assessed chorioallantoic fusion status by both the relative sliding motion of vascularized allantois against the overlying chorion in live-imaging (Sup-Mov.2; Sup-Mov.3) and by physical separation of the allantois and chorion after dissection. At the beginning of fifth day of chick development (~HH24; E4.0), chorioallantoic fusion was readily observed (Fig.2A). Statistical analysis showed a clear correlation between the embryo's developmental stage, allantoic size and chorioallantoic fusion status (Fig.2B). Based on these observations, we divided early chorioallantoic fusion process into two phases: a primary phase of chorioallantoic contact, transiting from no physical contact to physical contact, accompanied with sliding motion between interacting chorion and allantois (Sup-Mov.2) (E3.75-E4); and a secondary phase of physical fusion, transiting from physical contact to tissue fusion with reduced or no sliding motion between the chorion and allantois in the fused areas (Sup-Mov.3) (E4-E4.25). Taken together, our data showed that chicken CAM formation was achieved in a 12-hr window between E3.75 and E4.25, and that a brief contact of less than 6-hrs was sufficient to allow fusion to be established irreversibly. These observations suggested that chorioallantoic fusion is mediated by contact-based molecular signaling and subsequent cell morphological changes.

Electron microscopy analysis reveals chorionic and allantoic tissue organization at the primary phase of chorioallantoic fusion

Our time-lapse imaging (Sup-Mov.1) showed that initiation of chorioallantoic fusion coincided with the breakdown of vitelline membrane, an acellular protective layer covering the oocyte both before (as the

inner vitelline membrane) and after (as the outer vitelline membrane) fertilization. Avian inner vitelline membrane is similar in its function and composition to mammalian zona pellucida (Mann, 2008). Its breakdown, like mammalian blastocyst hatching, indicates maturation of the chorionic ectoderm as a protective epithelium. Our dye injection data suggested that the allantoic endoderm has also reached a mature epithelial status before fusion. These two protective layers likely maintain their fully-epithelial status during and after CAM formation. To investigate which chorioallantoic cellular lineage(s) are the main mediators of fusion, we first performed electron microscopy analysis of stage HH23/24 embryos (the primary phase of CAM fusion as defined in the previous paragraph) when the chorion and allantois had come into contact, but before fusion was established. The overall tissue organization of the chorion and allantois at this stage is shown in Fig.3A (semi-thin section; toluidine blue-stained) and Fig.3B (electron microscopy image). The allantois had a more complex tissue organization. Its endoderm layer had a smooth apical surface and a jagged basal one (Fig.3A,B). Its mesoderm components could be grouped into four cellular lineages based on their morphology: the blood cells, vascular endothelial cells, mesenchymal cells and a layer of mesoderm cells that cover the entire allantois (referred to as allantoic mesothelial cells) (Fig.3A,B).

Electron microscopy data showed that chorionic ectoderm cells had apical tight junctions (Fig.4A,B; black arrows), adherens junctions (Fig.4B white arrow) and basement membrane (Fig.4A,C,E,F; arrowheads), indicative of a mature epithelial organization. Chorionic ectoderm cells had a pseudostratified arrangement (Fig.4A-F, summary in Fig.4G). However, each ectoderm cells had apical and basal surfaces and its apicobasal axis spanned the entire thickness of the ectoderm, indicating that these cells had a special, interdigitating intercellular organization (Fig.4G). Below apical junctions between two chorionic ectoderm cells, neighboring cell membranes were arranged in a zigzagged pattern (Fig.4B,C) with additional adherens junction-like structures (Fig.4B,C,D white arrows) anchoring juxtaposed membranes. Chorionic mesothelial cells also formed intercellular junctions (Fig.4F arrow). These cells had protrusions

both apically (coelomic space side) and basally (chorionic ectoderm side), and did not have their own basement membrane (Fig.3A,B; Fig.4A,E,F). On the allantoic side, its mesothelial cells showed relatively smooth apical surface (Fig.3; Fig.5A), except in cells (Fig.5I arrows) which had been in contact with the chorionic side. Allantoic mesothelial cells had apical tight junctions (Fig.5A,B,C arrows), adherens junctions (Fig.5B,C arrowheads) and basement membrane (Fig.5D arrows). Allantoic endoderm cells exhibited stereotypic epithelial organization, with tight junctions (Fig.5E black arrow), adherens junctions (Fig.5E white arrow) and basement membrane (Fig.5E,F arrowheads). Between allantoic mesothelial cells and allantoic endoderm cells, as seen in semi-thin and electron microscopy images (Fig.3), additional mesoderm cell populations included blood cells (Fig.3), endothelial cells (Fig.3; Fig.5G,H) and allantoic mesenchymal cells (Fig.3), the last of which may be composed of heterogenous sub-populations.

Taken together (Fig.5J), our electron microscopy data suggested that at peri-fusion stage, the chorionic membrane is composed on a one-cell-thick chorionic ectoderm layer with a complex, previously undescribed epithelial organization, and a one-cell-thick mesothelial cell layer of partially polarized, epithelial-like organization. The allantoic membrane is composed of an inner endoderm layer of mature, cuboidal epithelial organization, a covering layer of epithelialized mesothelial cells, and between these two layers of epithelia, circulating blood cells, mature endothelial cells and mesenchymal cells of potentially heterogenous lineages.

Immunofluorescence analysis reveals characteristic cellular markers for epithelial structures during chorioallantoic fusion

To validate electron microscopy-based findings, we performed immunofluorescence analysis of chorionic and allantoic tissues from HH23 embryos (at the beginning of chorioallantoic contact). Laminin, the basement membrane marker (Nakaya et al., 2008), was strongly positive at the basal side of the chorionic

ectoderm cells (Fig.6B,D; Fig.6E arrow) and allantoic endoderm cells (Fig.6B,D; Fig.6F arrow), and moderately positive underneath allantoic mesothelial cells (Fig. 6B,D; Fig.6F white arrowhead). Vimentin (a mesenchymal marker) (Yang et al., 2020), however, was positive not only in allantoic mesenchymal cells (Fig.6C; Fig.6F black arrowheads), as expected, but also in chorionic mesothelial cells (Fig.6C; Fig.6E white arrowhead indicating mesothelial cells, black arrowhead indicating Vimentin positivity), and weakly positive in allantoic mesothelial cells (Fig.6F white arrowhead). E-cadherin, a canonical adherens junction marker (Nakaya et al., 2013; Nakaya et al., 2008), was highly expressed in chorionic ectoderm cells (Fig.6I,J) and allantoic endoderm cells (Fig.6L,N), but not in either chorionic or allantoic mesothelial cells (Fig.6I,J,L,N). ZO-1, a tight junction marker (Hamidi et al., 2020; Nakaya et al., 2008), was detected in both the chorionic ectoderm and chorionic mesothelial cells (Fig.6H,J), and in the allantoic endoderm cells, allantoic mesothelial cells and allantoic vascular endothelial cells (Fig.6M,N). Taken together (Fig.6O), our immunofluorescence data suggest that the chorionic ectoderm and allantoic endoderm cells are of stereotypic epithelial organization, and that the allantoic mesothelial cells are of full epithelial organization, but without expressing the canonical E-cadherin. The chorionic mesothelial cells are of a mixed epithelial (ZO-1 positive, stable cell-cell junctions under electron microscopy) and mesenchymal (Vimentin positive and Laminin negative) characteristics.

Chorioallantoic fusion does not require allantoic circulation or allantoic size increase

Close apposition of two mesothelial cell layers is common in development and adult homeostasis. In most such cases, however, fusion does not take place automatically after contact. For example, yolk sac splanchnic mesoderm is covered with a mesothelial layer as in the allantois, and is in contact with chorionic mesothelium for several days, without resulting in fusion, before this contact is displaced by the growing allantois and expanding chorioallantoic membrane. In the adult, mesothelial contact, involving

mesothelial layers lining body cavities, is essential for visceral organs' function, yet fusion is actively prevented, failure of which, e.g., as a consequence of surgery or dialysis, leads to human diseases (Mutsaers et al., 2015). We therefore investigated, at the tissue level, the essential parameters for chorioallantoic fusion.

Because in normal development, chorioallantoic fusion coincides with the phase of rapid size increase of the allantois, we asked whether fusion could still occur if allantois growth was prevented. We first performed chick/chick allantois graft, in which we used pre-fusion donor allantoides and equivalent stage host embryos. Graft allantois was collected by gentle excision with a pair of spring scissors at the connection between the donor allantois and the donor embryo. The collected, spherical, donor allantois was transplanted into the host extraembryonic coelomic cavity through a small slit cut in the host chorion, away from the final graft site. After overnight culture, the host allantois grew and established chorioallantoic fusion (Fig.7A), whereas the grafted allantois did not grow in size (Fig.7A,B) or re-establish circulation (Fig.7B). Yet, the fusion between the grafted allantois and the host chorion proceeded (9/15) (Fig.7B). Those grafted allantois that failed to fuse with the host chorion were invariably sunk in the extraembryonic coelomic cavity, possibly due to minor damage to the allantois during graft. When grafted allantois was in contact with the host allantois, blood flow could be re-established through vascular fusion of the two allantoides (Fig.8; Sup-Mov.4). In such cases, a rapid expansion of the graft allantois could be observed after vascular fusion (Fig.8; Sup-Mov.4). however, chorioallantoic fusion could take place regardless of whether allantoic circulation was re-established or not. This observation was confirmed by performing allantois graft experiments using quail donor allantois (20/26) (Fig.7H-K), or by in vitro assembly of isolated allantois and chorion tissues (13/16) (Fig.7C-G). TUNEL staining suggested that apoptosis was not involved in CAM fusion (CAM: Fig.7Q; limb-bud positive control: Fig.7R). These data suggested that the avian chorion and allantois have an intrinsic ability to initiate fusion (Fig.7S), likely through reciprocal signaling between two mesothelial layers, independent of allantoic circulation or

allantoic size increase. The allantoic size increase however, appeared to be the direct consequence of allantoic circulation, suggesting that content within the allantoic vesicle, at least during pre-fusion stages, is processed from the embryonic blood, rather than the embryonic mesonephros. In fused CAM, allantoic vascular elements (capillary vessels and vascular progenitor cells) will populate the chorionic mesoderm territory, and eventually also the chorionic ectoderm territory for efficient oxygen exchange. Supporting this, we detected mixed chorionic and allantoic mesoderm cells in chick/quail chimeric CAM (Fig.7L-P) soon after the fusion. Further studies will be needed to understand molecular regulation of the transition from an epithelial allantoic mesothelium and a partially epithelial chorionic mesothelium, before chorioallantoic fusion, to mesenchymal-shaped CAM mesoderm cells.

Conservation of chorioallantoic fusion in other amniotes, with a special discussion on origin of primate placentas

Phylogenetically speaking, all amniotes have conserved embryonic and extraembryonic tissue organization (Mossman, 1987; Sheng and Foley, 2012). The chorion is formed as the developing embryo is enclosed by the amniotic membrane (Fig.10 bottom), a structure that defines this group of vertebrate animals and ensures an aqueous environment for land-developing vertebrate embryos. As the external boundary of an amniote embryo, the chorion is the interface for fetal-environmental or fetal-maternal interactions, including the supply of oxygen and nutrients and the disposal of metabolic waste. The allantois is the main organ for metabolic waste storage in birds and reptiles, and through its fusion with the chorion, for oxygen supply in most amniote embryos and nutrient supply in viviparous squamates (snakes and lizards) and all mammals except for the marsupials. The marsupials use primarily chorio-vitelline placentas for feto-maternal interactions, although all marsupial embryos have an allantois and some also have a fused chorioallantoic membrane (Carter, 2021; Freyer et al., 2003). Among the eutherian

mammals, phylogenetic analysis has identified four major groups (Springer et al., 2004): the Afrotheria (e.g., elephants), Xenarthra (e.g., armadillos), Laurasiatheria (e.g., bats and pigs) and Euarchontoglires (e.g., primates, rodents and rabbits). The first three groups have their placentas derived from the CAM, involving a chorioallantoic fusion process similar to what we have described in this work (Mossman, 1987). Among the Euarchontoglires, Lagomorpha (rabbits, hares and pikas) (Hassan and Viebahn, 2017; Mossman, 1987) also undergoes chorioallantoic fusion as reported here, as is the case with basal primates (including flying lemur, lemur, loris, galago) (Hill, 1932; Mossman, 1987). Rodents also involve mesothelial cells during chorioallantoic fusion (Downs, 2002; Downs and Gardner, 1995), although in this group contribution of endoderm to pre- and peri-fusion allantois is highly variable, from having no endoderm cavity (but with endoderm-derived allantoic rod cells) in allantoic outgrowth in mice (Fig.10) (Downs and Rodriguez, 2020), to having a well-formed, endoderm-enclosed allantoic cavity in squirrels (Luckett, 1971; Mossman, 1987).

Morphogenetic process leading to chorioallantoic fusion in haplorhini (a clade of primates to which our own species belong) is less clear. This is mainly due to scarcity of early-stage embryo samples in human and other anthropoid species, but is also complicated by two special features in early human/anthropoid development: the body stalk and presence of a large number of extraembryonic mesoderm/mesenchymal cells before primitive streak formation. The body stalk connects the embryo proper with the chorionic ectoderm (trophoblasts) (Mossman, 1987; Vögler, 1987) and is composed of mesoderm-like cells formed when epiblast cells transition from a partially epithelial and partially mesenchymal status to a fully epithelial one (Sheng, 2015, 2021; Yang et al., 2020). From histological sections, a significant number of such mesoderm-like cells, populating the body stalk and covering the amniotic and chorionic ectoderm, are already present before initiation of primitive streak-associated gastrulation and epithelial to mesenchymal transition. Although these cells resemble the hypoblast in cellular architecture and gene

expression patterns (Luckett, 1978; Nakamura et al., 2016; Sasaki et al., 2016), their origin, e.g., from either the epiblast, hypoblast, or both, remains to be clarified through direct lineage tracing analysis.

Allantoic formation in anthropoids is presumably initiated by endoderm outgrowth into this pre-existing body stalk territory (Vögler, 1987). For ethical and technical reasons as mentioned above, systematic analysis of allantoic and chorioallantoic membrane formation in anthropoids is lacking. We analyzed early stage (Carnegie Stage 8) (O'Rahilly and Muller, 2010) human embryo sample (Fig.9A-C) and somewhat more advanced stage (E22) (Nakamura et al., 2016) macaque embryo sample (Fig.9D-H). Endoderm-enclosed allantoic cavity/diverticulum was observed in allantoic stalk in both species (Fig.9A-C,D,E). Interestingly, in the human sample, which is at an earlier developmental stage when allantoic endoderm diverticulum just started to invade into the body stalk, a mesothelium-like layer covered a portion of the stalk, suggesting that morphological heterogeneity exists in human body stalk mesoderm cells and that human allantoic growth is associated with, but distinguishable from the pre-existing body stalk. The body stalk becomes allantoic stalk when allantois-associated endoderm expands into much of the body stalk territory (Fig.9D,E; arrows), bringing with it vascular mesoderm cells which eventually connect embryonic and placental circulatory networks. Cells of vascular endothelial morphology were observed more abundantly in allantoic stalk and in chorionic mesoderm territory adjacent to allantoic stalk (Fig.9E), suggesting that allantois-associated mesoderm makes a major contribution to placental vasculature. Supporting this, mesenchymal cells located in chorionic villi, prior to vascular infiltration, did not exhibit prominent vascular morphology (Fig.9H). However, in the macaque embryo, chorionic mesoderm cells lining the extraembryonic coelomic cavity appeared to be capable of differentiating into vascular endothelial cells (Fig.9G; red arrowhead). This is different from what we observed in avian embryos, where chorionic mesothelial cells did not make any obvious contribution to the vascular cell lineage prior to CAM fusion.

Conclusions

Chorioallantoic fusion generates the embryonic respiratory organ in birds and reptiles and the placenta in mammals. In this work, we carried out detailed morphological, cellular and comparative analyses of chorioallantoic fusion. Our data suggested that in amniotic vertebrates, including in most of mammalian groups, chorioallantoic fusion involves cross-talk between two mesothelial layers, one covering the allantoic vascular mesoderm and the other the chorionic ectoderm. The fusion process is rapid, does not require allantoic circulation or size increase, and involves partial epithelial-mesenchymal transition of two mesothelia. Identifying molecular regulators of chorioallantoic fusion and mesothelial epithelial-mesenchymal transition in future studies will help us understand underlying mechanisms of human placenta defects and mesothelial-related human diseases.

Acknowledgements

We would like to thank support from Takeda Science Foundation (to GS), JSPS (Kahenhi 18H02452 and 21H02490 to GS and 18K06265 to HN), Kumamoto University IRCMS (to GS) and Grant - in - Aid for Transformative Research Area B (JP20B302, 20H05761 to TN). We are grateful to Drs Hideyuki Tsuchiya and Chizuru Iwatani and other animal care staff (Research Center for Animal Life Science, Shiga university of Medical Science) for their assistance in sampling the macaque materials. We would also like thank Dr Akihiko Yoshizawa and the staff (Center for Anatomical, Pathological and Forensic Medical Research, Kyoto University Graduate School of Medicine) for the assistance in macaque histological analysis.

Materials and Methods

Embryology and Imaging

Fertilized chicken and quail eggs were purchased from Shimojima Farm (Kanagawa, Japan) and Motegi Farm (Saitama, Japan), respectively. Eggs were incubated at 38.5 °C to desired stages. For time-lapse imaging of *in ovo* development, we used heated incubator chamber (Fig.1B) (manufactured by Matsunami Glass IND LTD., Japan) and Olympus SZX16 microscope fitted with Olympus DP72 camera. For allantois graft experiment, the donor allantois (from HH23/24) was excised at the proximal side (where the allantois connects to the embryo) and was allowed to heal. A small slit, the length of which was smaller than the diameter of graft allantois, was made on host chorionic membrane. Graft allantois was then carefully inserted through the slit and should be floating in extraembryonic coelomic cavity space if its integrity was intact. The graft allantois was moved gently away from the open slit (which would heal after overnight incubation) to allow close physical contact between the graft allantois and host chorion. The status of fusion was analyzed after overnight incubation (12-24 hours). For *in vitro* chorioallantoic fusion experiment, pre-fusion allantois and chorion were isolated separately, and were assembled and stabilized using fine insect pins (Fig.7C) on semi-solid agarose (0.8-0.9%) in Tyrode's saline. Mesothelial side of the chorion was placed facing the mesothelial side of the allantois, and assembled chorion and allantois were incubated at 38.5 °C in humidified container.

Immunostaining

For immunofluorescence or immunohistochemistry analysis, the following primary antibodies were used: E-cadherin (BD Transduction Lab; #610181), ZO-1 (Invitrogen; #40-2200), Laminin (Sigma; #L9393), Vimentin (DSHB; H5) and quail specific marker (DSHB; QCPN). Alexa Fluor secondary antibodies (Alexa flour 488 and 568; Invitrogen) were used for multicolour detection. Immunofluorescence images were

captured using Keyence Fluorescence Microscope BZ-X800 and processed using Fiji image processing package (Schindelin et al., 2012). Immunohistochemistry images were acquired using Olympus BX52 with Olympus DP70 camera.

Electron Microscopy

For electron microscopy analysis, samples of chicken chorion and allantois were prepared according to standard protocol. Briefly, isolated tissue samples were fixed overnight at 4 °C with 2.5% glutaraldehyde and 2% paraformaldehyde in 0.1 M phosphate buffer, postfixed in 1% OsO_4 on ice, and stained en bloc with 1.5% uranyl acetate. After embedding in epoxy resin, ultrathin sections were cut and stained with uranyl acetate and lead citrate. Specimens were examined with a transmission electron microscope (H-7700, Hitachi).

Human Embryo Section

Human embryo section slide was from the Kyoto Collection of Human Embryos, a projected initiated in 1961 by Dr. Hideo Nishimura in Kyoto University and currently comprises over 44,000 human embryo samples (Yamaguchi and Yamada, 2018). The specimen number for images shown in Figure 9 is #27423 and developmental stage of this specimen is CS8.

Cynomolgus macaque sample collection and histology

Experimental procedures using cynomolgus macaques were approved by the Animal Care and Use Committee of Shiga University of Medical Science. Post-implantation Cynomolgus macaque embryo at

E22 were generated by oocyte collection, intracytoplasmic sperm injection, culture of pre-implantation embryo, embryo transfer into female recipients and recover of embryo by cesarean section under full anesthesia, as described previously (Nakamura et al., 2016; Sasaki et al., 2016; Suemori et al., 2001; Yamasaki et al., 2011). The embryos were fixed in 4% PFA/PBS at 4°Covernight and embedded in paraffin. The sample was serially sectioned at a thickness of 3 micro-meter on a microtome and stained with hematoxylin and eosin (ScyTek, HAE-1). The images were acquired by Nanozoomer virtual slide scanner (Hamamatsu Photonics).

TUNEL assay

Whole mount detection of apoptotic cells was perfomed using in situ apoptosis detection kit (Takara; #MK500) in combination with anti-Fluorescein-AP, Fab fragments (Roche; #11426338910).

Figure Legends

Figure 1: Gross morphology and timing of chorioallantoic fusion in chick development

A: Schematic view of an amniote embryo, including its germ layer organization and relationship between its intra-embryonic and extra-embryonic structures. Red: mesoderm derivatives. Gray: ectoderm and endoderm derivatives**. B,C:** Custom-built incubator for time-lapse imaging. Eggshell is opened from one side, exposing the developing embryo. The incubator is humidified by a small reservoir of water at its base and heated from the top. The glass is heated to prevent water condensation (C). The incubator is placed under a stereomicroscope (e.g., Olympus SZX16) for long-term time-lapse imaging. The water reservoir is refilled daily to maintain humidity. **D:** A HH21 embryo, showing its growing allantois (artificially injected with fast green dye). **E:** Still images captured from time-lapse movie (Sup-Movie 1), showing rapid increase in allantoic size from HH18 to HH26.

Figure 2: Correlation of chorioallantoic fusion and allantois size in chick development

A: Fusing chorion (ch) and allantois (al), showing both the ongoing fusion (CAM) and unfused territories. **B:** Average size and fusion status of the chorion and allantois, with respect to embryo's developmental stage.

Figure 3: Histological and electron microscopy analyses of chorionic and allantoic tissues at the onset of fusion.

A: Toluidine blue-stained semi-thin (0.5 μm) section of chorionic and allantoic tissues. Germ layer composition as indicated. Chorion contains ectoderm and mesoderm (mesothelium) layers. Allantois contains endoderm and mesoderm layers. The allantoic mesoderm is heterogenous, containing

mesothelial, endothelial, blood and mesenchymal cells. **B:** Transmission electron microscopy showing overall organization of the chorionic and allantoic tissues. Scale bar: 25 μm in A and 8 μm in B. Cell lineages are indicated by white (in A) and black (in B) arrowheads.

Figure 4: Electron microscopy analysis of the chorion.

A: The chorion contains the ectoderm and mesoderm layers (both indicated by brackets). Arrowhead: ectodermal basement membrane. Arrow: ectodermal apical junctions. **B:** Magnified view of apical junction region shown in A. TJ: tight junction; AJ: adherens junction. Below apical junctions, chorionic ectoderm cell membranes are arranged in an interdigitating pattern, anchored by additional adherens junction-like structures (white arrow labelled as AJ-like in **B,C,D**). **E:** Chorionic ectoderm cells also exhibit a complex pattern in their basal side. **F:** Under chorionic ectoderm, a basement membrane (arrowheads) is clearly visible. Chorionic mesothelial cells do not have detectable basement membrane of their own, but intercellular junctions are present. **G:** Schematic view of cellular organization of the chorionic ectoderm. **Top**: Schematic representation of ectoderm cells shown in panel **A**. **Bottom:** Chorionic ectoderm cells are unilaminar, with complex intercellular organization possibly to fulfill physiological roles of the chorionic ectoderm (e.g., by providing a strong physical barrier, preventing water and heat loss, and facilitating oxygen uptake).

Figure 5: Electron microscopy analysis of the allantois.

A-D: Allantoic mesothelial cells have clear cell-cell junctions (arrows in **A**), including tight junctions (arrows in **B,C**) and adherens junctions (arrowheads in **B,C**), and basement membrane (arrowheads in **D**). **E:** Allantoic endoderm cells are stereotypic epithelial organization, with tight junction (black arrow),

adherens junction (white arrow) and basement membrane (black arrowhead). **F:** Magnified view of endodermal basement membrane region indicated by arrowhead in **E**. **G,H**: Vascular endothelial cells in allantoic mesoderm compartment are also connected by tight junctions (black arrows). **I**: in some allantoic mesothelial cells, different from those shown in panel A, numerous apical filopodia-like structure are seen. These filopodia likely reflect changes in allantoic mesothelial cells induced by contact with the chorionic tissue, in preparation for fusion. **J:** Summary of cellular organization, including their heterogeneity and polarity), in chorionic and allantoic tissues.

Figure 6: Immunofluorescence analysis of chorionic and allantoic tissues at the onset of fusion.

A-F: Chorionic and allantoic tissues from HH23 embryo stained for DAPI (**A**), Laminin (**B**) and Vimentin (**C**), superimposed in (**D**). Magnified views for chorion (**E**) and allantois (**F**). **G-J:** Chorionic tissue from HH23 embryo stained for DAPI (**G**), ZO-1 (H) and E-cadherin (E-cad) (**I**), superimposed in **J**. **K-N**: allantoic tissue from HH23 embryo stained for DAPI (**K**), E-cad (**L**) and ZO-1 (**M**), superimposed in **N**. **O**: Summary of immunofluorescence analysis. Scale bar: 50 μm in panels A-D, G-N; 25 μm in panels E and F.

Figure 7: Allantoic graft in vivo and chorioallantoic fusion in vitro

A,B: Graft chick allantois fuses with host chorion. **B** is magnified view of **A**. Donor allantois was inserted into host extraembryonic coelomic cavity through a small slit in host chorion. After overnight growth, the host allantois grew in size, whereas the graft allantois (arrows) did not. But chorioallantoic fusion (host chorion and donor allantois) still took place. **C-G**: Chorioallantoic fusion in vitro. **C,D**: schematic diagram (**C**) and example (**D**) of isolated chorionic and allantoic tissues put together in vitro. **E**: After 12 hours, fusion was observed. At this point, however, the fusion was still weak and these two tissues could still be

separated by peeling. **F,G**: After 24-hours, fusion was firmly established. **H-K**: Quail/chick (graft/host) allantoic graft. **H**: two graft allantois (quail, arrows) in chick host. The host allantois is labelled as such. **I-K**: after QCPN staining, two quail allantois could be clearly distinguished (I; and magnified view in **J** and **K**). **L-P**: Section view of quail allantois after QCPN staining. The fused chorioallantoic membrane (**L,M,O**) contains both quail (stained) and chick cells (unstained). The unfused allantois contains all quail cells (**L,M**). At the edge of fusion, a complex pattern of cell mixing (**L,N,P**) could be observed. **Q**: TUNEL staining of HH23+ CAM, showing no or very few apoptotic cells. **R**: TUNEL staining of the forelimb bud of the same embryo, showing prominent apoptosis in apical ectoderm ridge, as previously reported (Fernandez-Teran et al., 2006). **S**: Schematic diagram of how chorioallantoic fusion is regulated. Allantoic circulation is critical for allantoic size expansion, but does not function as the primary driver for fusion. Chorionic mesoderm does not contain vascular endothelial cells by itself, and vascular progenitors originated from allantoic mesoderm invades into chorionic mesoderm territory, and eventually to intra-chorionic ectoderm territory for efficient oxygen uptake. Reciprocal signaling between allantoic and chorionic mesothelial cells are considered to be the main driver for chorioallantoic fusion.

Figure 8: Allantoic circulation leads to allantoic size increase.

A: Graft allantois was labeled with injected fast green dye and subject to time lapse imaging. Without circulation, the graft allantois did not expand in size. In some cases, the mesoderm components of the graft allantois and host allantois fused (e.g., at 6h in A), resulting in rapid expansion of the graft allantois. **B:** This is more clearly shown when two graft allantoides, one having vascular fusion with the host allantois (starting at 6.5h) and the other not. **C,D:** magnified views of 4.5h (C) and 8.5h (D) of the time-lapse sequence shown in **B**.

Figure 9: Chorioallantoic membrane fusion in human and macaque samples.

A-C: Carnegie Stage 8 human embryo (from Kyoto Human Embryo collection). **A** and **B** are two sections of the same embryo. **C** is magnified view of **B**. Allantoic endoderm diverticulum (shown in **A-C**) extends into the body stalk mesoderm. The body stalk exists before gastrulation is initiated. Mesenchymal cells in the body stalk represent those mesoderm cells that contribute to the majority of chorionic and amniotic mesoderm. The extension of allantoic endoderm diverticulum into the body stalk brings additional mesoderm cells generated through gastrulation to the body stalk, transforming body stalk into allantoic stalk. **D-H**: E22 macaque embryo. D: section view of embryo, with major extraembryonic tissues labeled. **E**: Magnified view of the allantoic stalk, showing central, endoderm-lined allantoic cavity space (arrows). **F**: Magnified view of the yolk sac. Arrows: yolk sac endoderm cells. Arrowheads: developing blood islands. **G**: Magnified view of amnion and chorion, in regions away from the allantoic stalk. Both amniotic ectoderm and amniotic mesoderm are one-cell-layer thick; whereas chorionic ectoderm contains both syncytial and cyto- trophoblasts and chorionic mesoderm is multi-cell-layered. Occasional cells with vascular endothelial-like morphology can be detected in chorionic mesoderm (red arrowhead). These endothelial-like cells appear to have formed in situ (i.e., are not derived from allantoic mesoderm). **H**: Chorionic villi have mesoderm core (non-vascular cells) surrounded by trophoblasts (cyto- and syncytial).

Figure 10: Comparative view of chorioallantoic membrane fusion in amniotic vertebrates.

Schematic diagram summarizing phylogenetic view of anatomical and functional conservation/diversification of chorioallantoic membrane. Red: mesoderm derivatives. Gray: ectoderm and endoderm derivatives.

Supplementary Movie Legends

Supplementary Movie 1:

Time-lapse movie of chick development from HH15 to HH27, taken at 5 minutes/frame for three days.

Supplementary Movie 2:

Real time movie of chicken allantois, after its contact with the chorion but before fusion is established.

Supplementary Movie 3:

Real time movie of chicken allantois, after fusion is established.

Supplementary Movie 4:

Time lapse movie of two graft chicken allantoides, one with vascular fusion with host allantois and the other not.

References

Carter, A.M. (2012). Evolution of placental function in mammals: the molecular basis of gas and nutrient transfer, hormone secretion, and immune responses. Physiol Rev *92*, 1543-1576.

Carter, A.M. (2021). The role of mammalian foetal membranes in early embryogenesis: Lessons from marsupials. J Morphol *282*, 940-952.

Coleman, J.R., and Terepka, A.R. (1972). Fine structural changes associated with the onset of calcium, sodium and water transport by the chick chorioallantoic membrane. J Membr Biol *7*, 111-127.

Downs, K.M. (2002). Early placental ontogeny in the mouse. Placenta *23*, 116-131.

Downs, K.M., and Gardner, R.L. (1995). An investigation into early placental ontogeny: allantoic attachment to the chorion is selective and developmentally regulated. Development *121*, 407-416.

Downs, K.M., and Rodriguez, A.M. (2020). The mouse fetal-placental arterial connection: A paradigm involving the primitive streak and visceral endoderm with implications for human development. Wiley Interdiscip Rev Dev Biol *9*, e362.

Fernandez-Teran, M.A., Hinchliffe, J.R., and Ros, M.A. (2006). Birth and death of cells in limb development: a mapping study. Dev Dyn *235*, 2521-2537.

Freyer, C., Zeller, U., and Renfree, M.B. (2003). The marsupial placenta: a phylogenetic analysis. J Exp Zool A Comp Exp Biol *299*, 59-77.

Hamidi, S., Nakaya, Y., Nagai, H., Alev, C., Kasukawa, T., Chhabra, S., Lee, R., Niwa, H., Warmflash, A., Shibata, T.*, et al.* (2020). Mesenchymal-epithelial transition regulates initiation of pluripotency exit before gastrulation. Development *147*.

Hassan, W., and Viebahn, C. (2017). A correlative study of the allantois in pig and rabbit highlighting the diversity of extraembryonic tissues in four mammalian species, including mouse and man. J Morphol *278*, 600-620.

Hill, T.P. (1932). Croonian lecture: the developmental history of the primates. Philosophical Transactions of the Royal Society of London B *221*, 45-178.

Hirota, S. (1894). On the Sero-Amniotic Connection and the Foetal Membranes in the Chick. The journal of the College of Science, Imperial University, Japan *6*, 337-370.

Hoshi, H., and Mori, T. (1971). The fine structure of the chorionic epithelium of chick embryo. Arch Histol Jpn *33*, 45-58.

Luckett, W.P. (1971). The development of the chorio-allantoic placenta of the African scaly-tailed squirrels (family Anomaluridae). Am J Anat *130*, 159-177.

Luckett, W.P. (1978). Origin and differentiation of the yolk sac and extraembryonic mesoderm in presomite human and rhesus monkey embryos. Am J Anat *152*, 59-97.

Mann, K. (2008). Proteomic analysis of the chicken egg vitelline membrane. Proteomics *8*, 2322-2332.

Mossman, H.W. (1987). Vertebrate fetal membranes : comparative ontogeny and morphology, evolution, phylogenetic significance, basic functions, research opportunities (New Brunswick, N.J.: Rutgers University Press).

Mutsaers, S.E., Birnie, K., Lansley, S., Herrick, S.E., Lim, C.B., and Prele, C.M. (2015). Mesothelial cells in tissue repair and fibrosis. Front Pharmacol *6*, 113.

Nakamura, T., Okamoto, I., Sasaki, K., Yabuta, Y., Iwatani, C., Tsuchiya, H., Seita, Y., Nakamura, S., Yamamoto, T., and Saitou, M. (2016). A developmental coordinate of pluripotency among mice, monkeys and humans. Nature *537*, 57-62.

Nakaya, Y., Sukowati, E.W., and Sheng, G. (2013). Epiblast integrity requires CLASP and Dystroglycan-mediated microtubule anchoring to the basal cortex. J Cell Biol *202*, 637-651.

Nakaya, Y., Sukowati, E.W., Wu, Y., and Sheng, G. (2008). RhoA and microtubule dynamics control cell-basement membrane interaction in EMT during gastrulation. Nat Cell Biol *10*, 765-775.

O'Rahilly, R., and Muller, F. (2010). Developmental stages in human embryos: revised and new measurements. Cells Tissues Organs *192*, 73-84.
Perez-Garcia, V., Fineberg, E., Wilson, R., Murray, A., Mazzeo, C.I., Tudor, C., Sienerth, A., White, J.K., Tuck, E., Ryder, E.J.*, et al.* (2018). Placentation defects are highly prevalent in embryonic lethal mouse mutants. Nature *555*, 463-468.
Romanoff, A.L. (1960). The extraembryonic membranes. In The avian embryo: structural and functional development (New York: The Macmillan Company), pp. 1041-1140.
Rossant, J., and Cross, J.C. (2001). Placental development: lessons from mouse mutants. Nat Rev Genet *2*, 538-548.
Sasaki, K., Nakamura, T., Okamoto, I., Yabuta, Y., Iwatani, C., Tsuchiya, H., Seita, Y., Nakamura, S., Shiraki, N., Takakuwa, T.*, et al.* (2016). The Germ Cell Fate of Cynomolgus Monkeys Is Specified in the Nascent Amnion. Dev Cell *39*, 169-185.
Schindelin, J., Arganda-Carreras, I., Frise, E., Kaynig, V., Longair, M., Pietzsch, T., Preibisch, S., Rueden, C., Saalfeld, S., Schmid, B.*, et al.* (2012). Fiji: an open-source platform for biological-image analysis. Nat Methods *9*, 676-682.
Sheng, G. (2015). Epiblast morphogenesis before gastrulation. Dev Biol *401*, 17-24.
Sheng, G. (2021). Defining epithelial-mesenchymal transitions in animal development. Development *148*.
Sheng, G., and Foley, A.C. (2012). Diversification and conservation of the extraembryonic tissues in mediating nutrient uptake during amniote development. Ann N Y Acad Sci *1271*, 97-103.
Springer, M.S., Stanhope, M.J., Madsen, O., and de Jong, W.W. (2004). Molecules consolidate the placental mammal tree. Trends Ecol Evol *19*, 430-438.
Steinmetz, H. (1930). Die Embryonalenentwick- lung des Blasshuhns (Fulcia atra) unter besonderer Berucksichtigung der Allantois. Morphol Jahrb *64*, 275-338.
Suemori, H., Tada, T., Torii, R., Hosoi, Y., Kobayashi, K., Imahie, H., Kondo, Y., Iritani, A., and Nakatsuji, N. (2001). Establishment of embryonic stem cell lines from cynomolgus monkey blastocysts produced by IVF or ICSI. Dev Dyn *222*, 273-279.
Vögler, H. (1987). Human blastogenesis : formation of the extraembryonic cavities (Basel ; New York: Karger).
Yamasaki, J., Iwatani, C., Tsuchiya, H., Okahara, J., Sankai, T., and Torii, R. (2011). Vitrification and transfer of cynomolgus monkey (Macaca fascicularis) embryos fertilized by intracytoplasmic sperm injection. Theriogenology *76*, 33-38.
Yang, J., Antin, P., Berx, G., Blanpain, C., Brabletz, T., Bronner, M., Campbell, K., Cano, A., Casanova, J., Christofori, G.*, et al.* (2020). Guidelines and definitions for research on epithelial-mesenchymal transition. Nat Rev Mol Cell Biol *21*, 341-352.

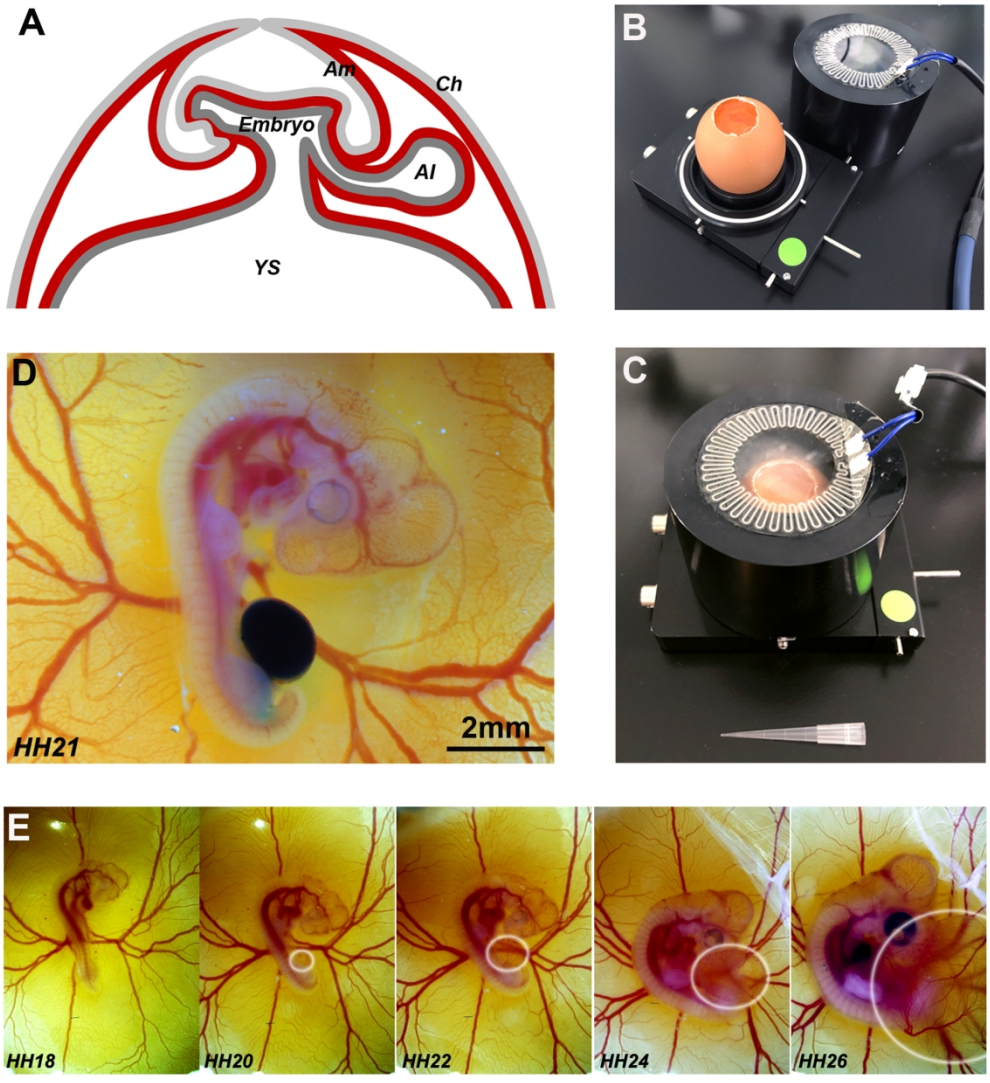

revision figure 1

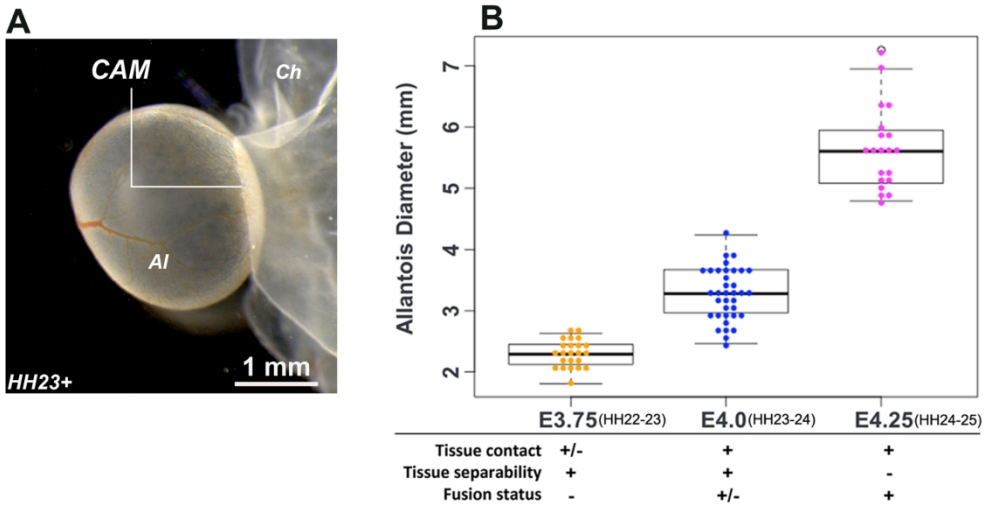

revision figure 2

165x88mm (300 x 300 DPI)

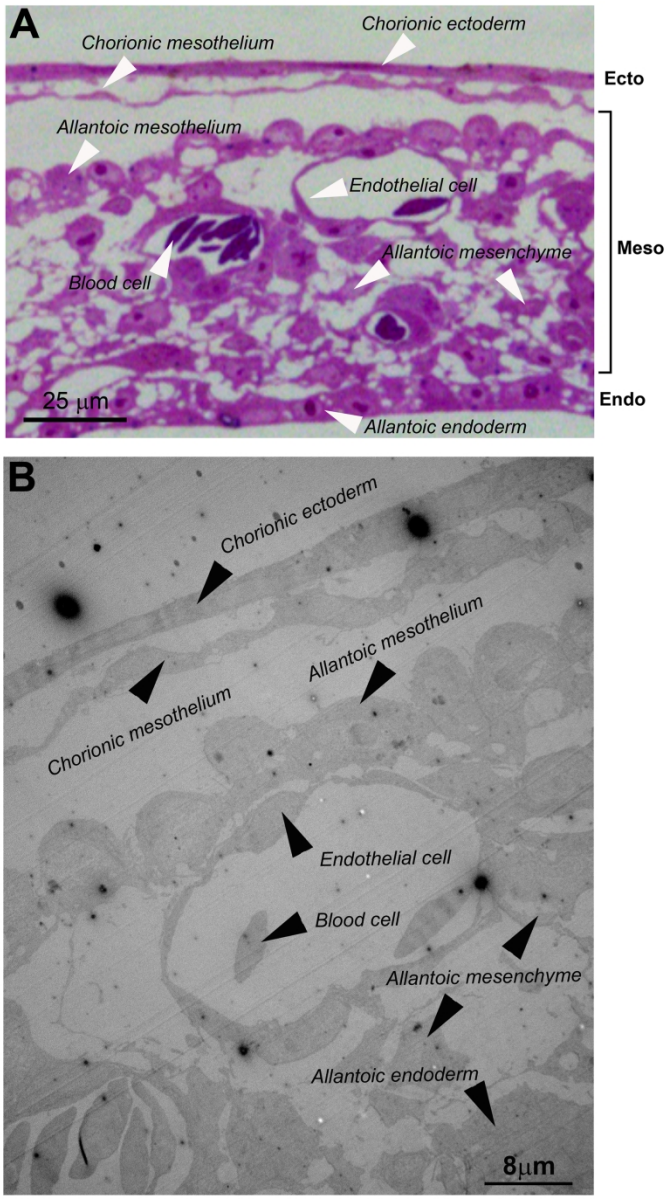

revision figure 3

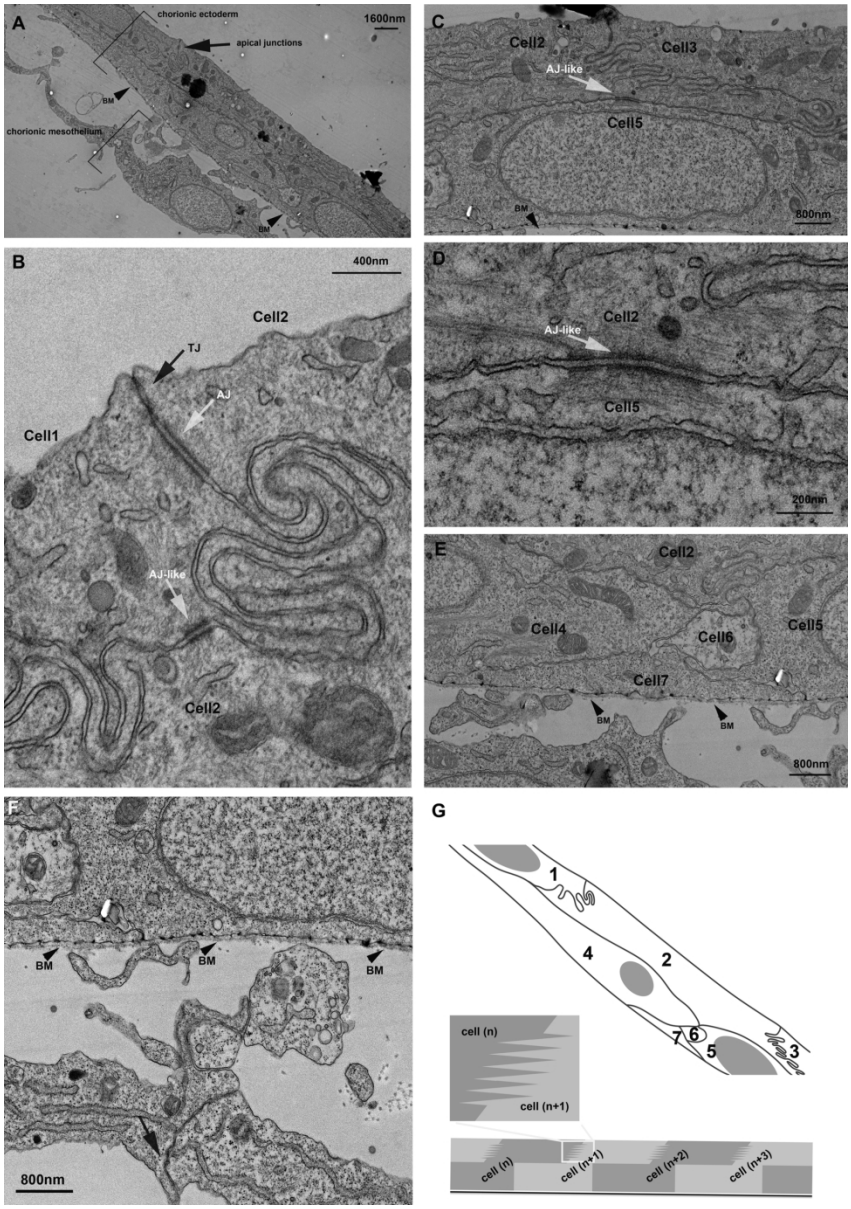

revision figure 4

165x234mm (300 x 300 DPI)

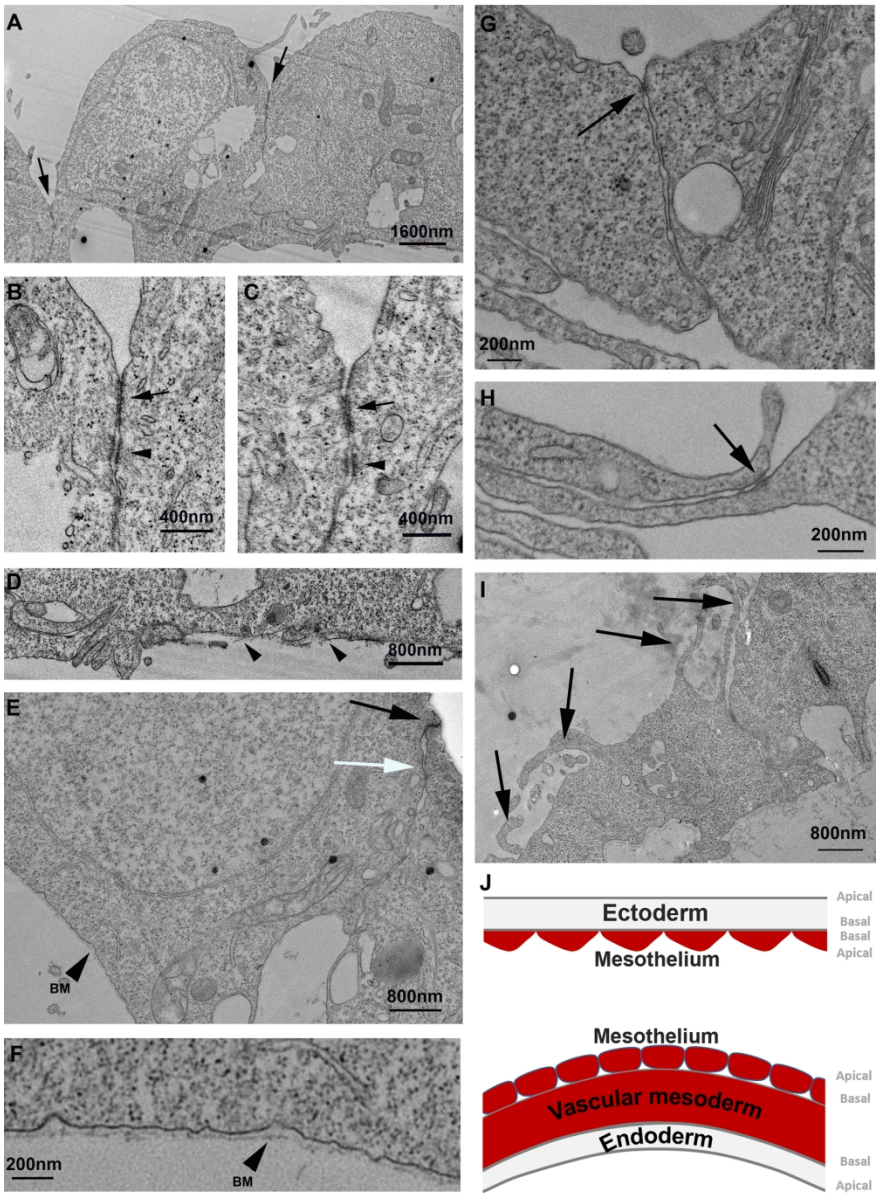

revision figure 5

165x226mm (300 x 300 DPI)

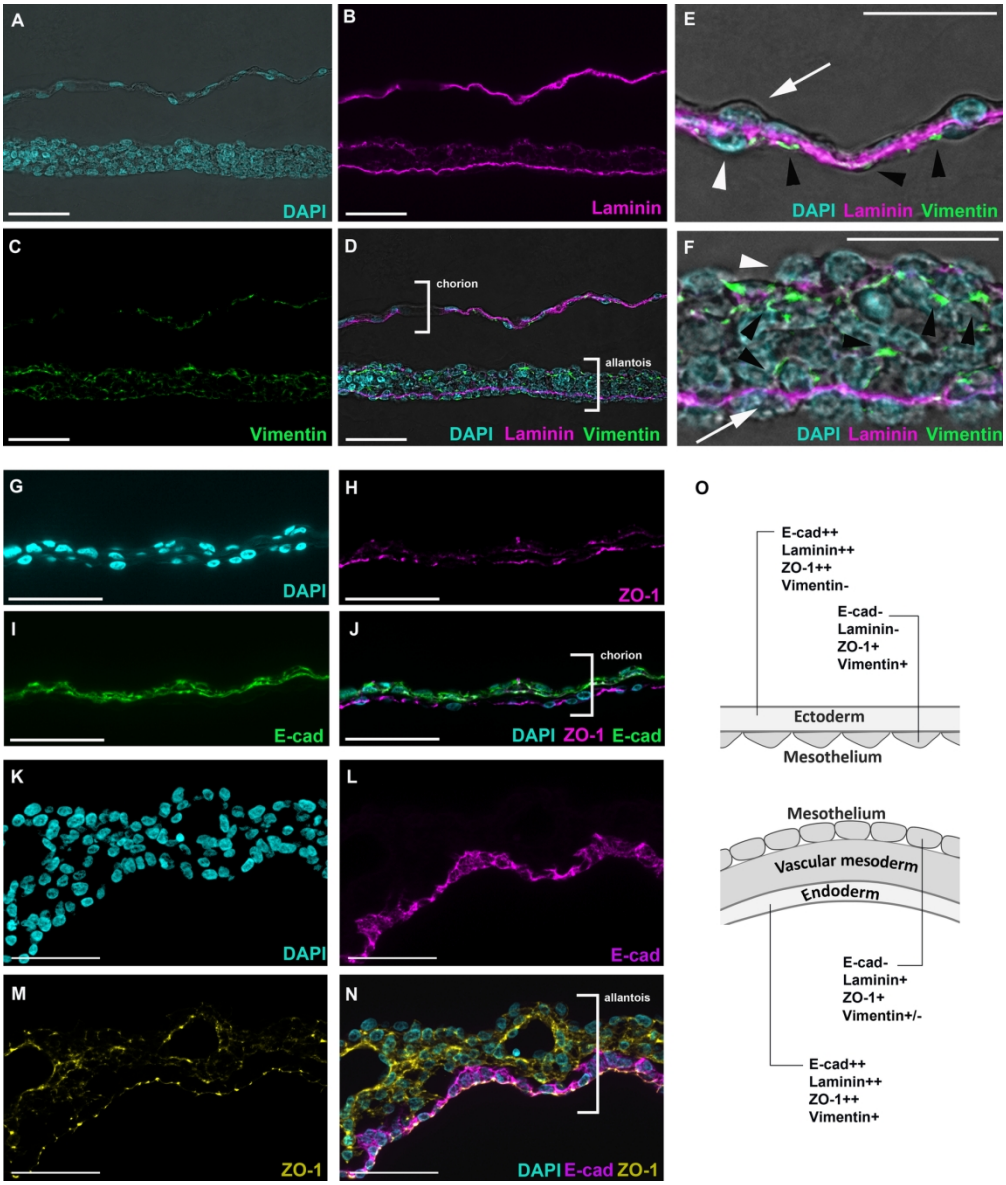

revision figure 6

165x194mm (300 x 300 DPI)

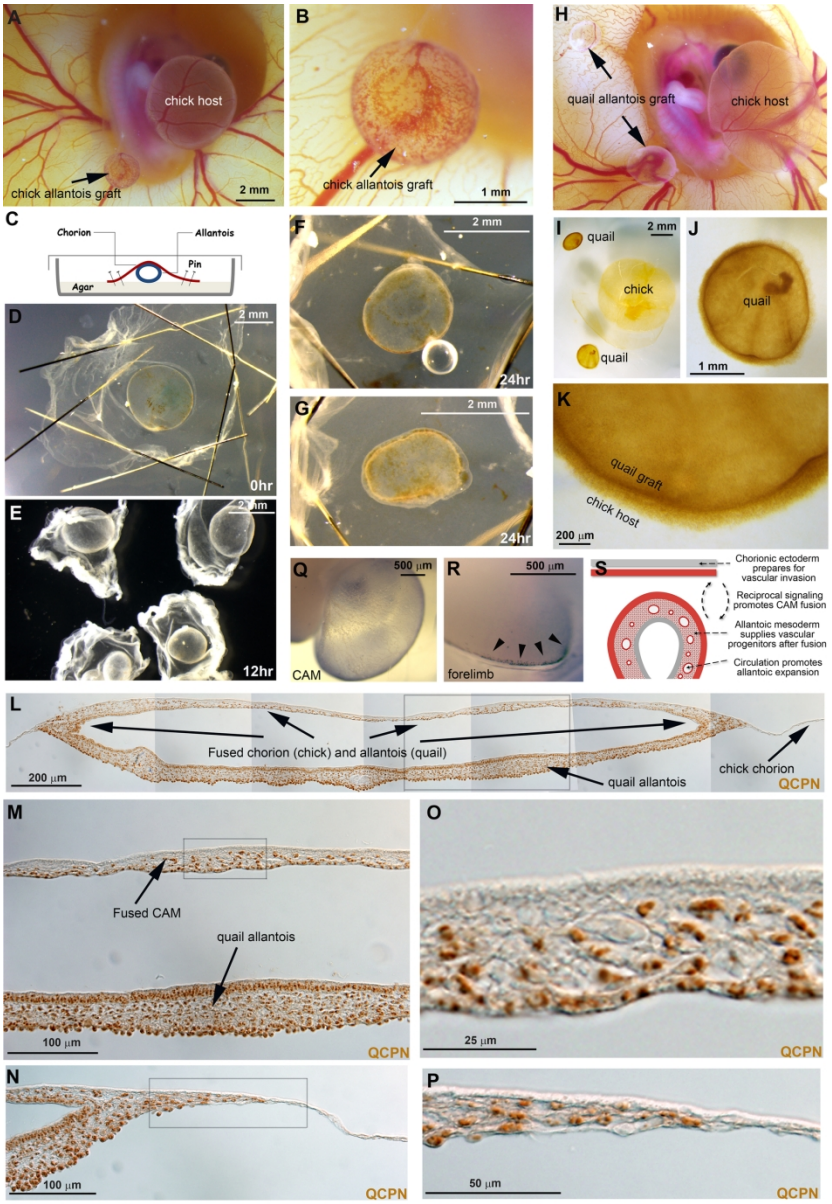

revision figure 7

165x238mm (300 x 300 DPI)

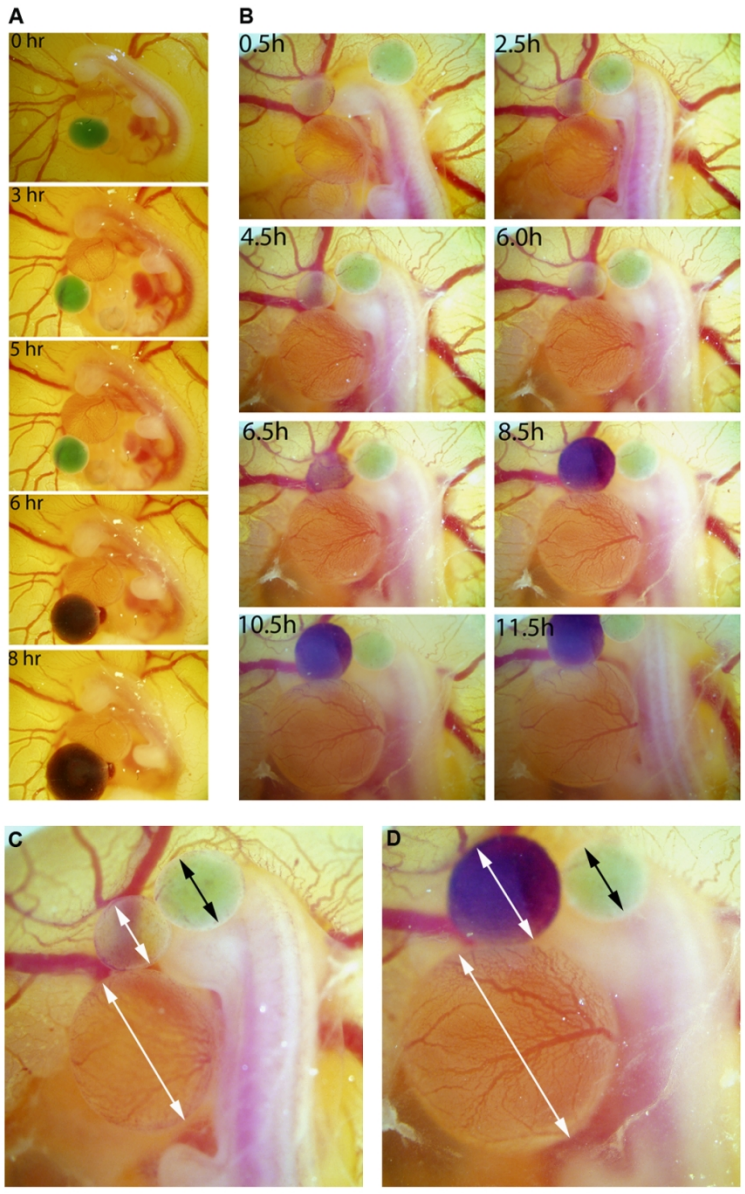

revision figure 8

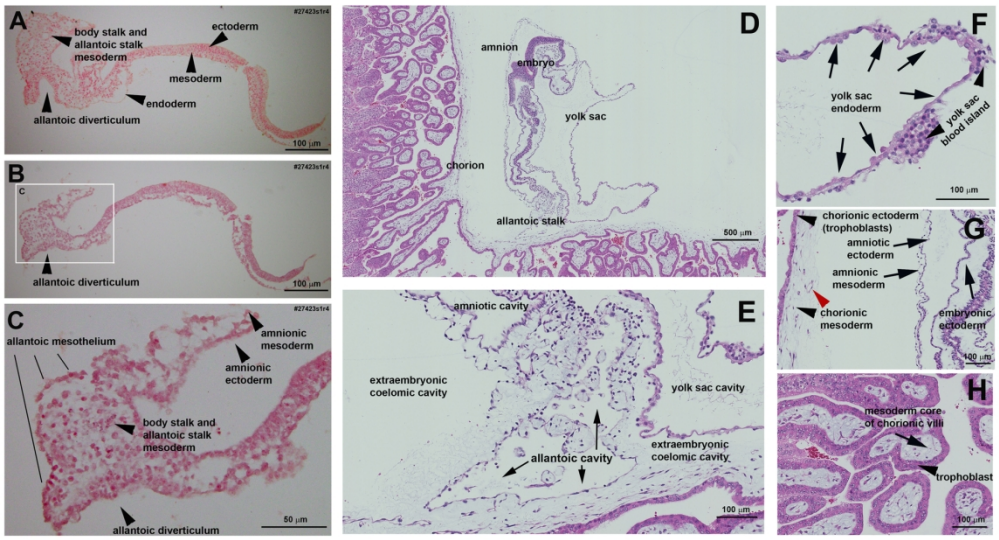

revision figure 9

165x89mm (300 x 300 DPI)

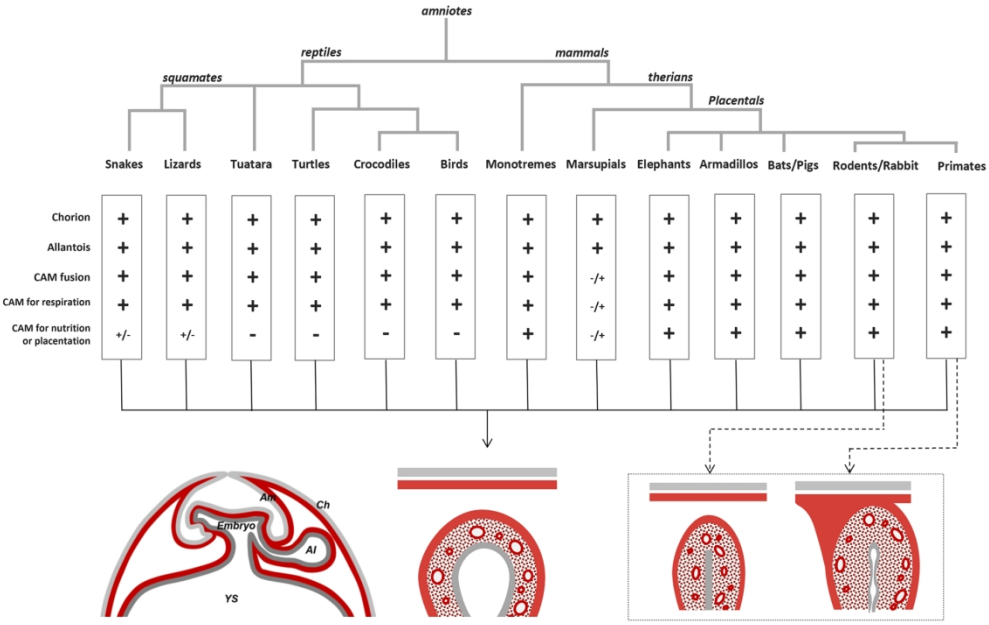

revision figure 10